ON-LINE APPENDIX

Supplemental Methods

Image Reconstruction and Coregistration. Na image raw data were reconstructed off-line by a custom-written Matlab script (MathWorks, Natick, Massachusetts). To reduce Gibbs ringing artifacts, a Hamming filter was applied. Contrast-enhanced T1-weighted images (T1 CE) were skull-stripped by the FSL Brain Extraction Tool (http://fsl.fmrib.ox.ac.uk/fsl/fslwiki/BET)[1] and served as individual reference images. T2-TSE, T2-FLAIR, and Na images were coregistered to this reference image by using an affine registration with 12 degrees of freedom as implemented in the FMRIB Linear Image Registration Tool (FLIRT, http://www.fmrib.ox.ac.uk/).[2] Two-dimensional overlays of Na-MR data onto anatomic ^{1}H-MR images were generated by using FreeSurfer (http://surfer.nmr.mgh.harvard.edu) freeview.[3]

Tissue Segmentation by using Ilastik. Ilastik uses machine learning techniques that consider information from all MR contrasts (Na and H) simultaneously, that is, it works on multimodal data. For segmentation of different tissue compartments (healthy tissue, whole tumor VOI, and CE tumor VOI), we used the Pixel-Classification workflow of the ilastik project (https://github.com/ilastik/). It is based on 10 random forests,[4] with 10 trees each that are trained in parallel and eventually merge into a single forest. Gini impurity is used as a split criterion, and the number of randomly chosen features at each split is proportional to the square root of the total number of features. Postprocessing of the pseudo-probabilities (that were obtained from the random forest predictions) ensued with a custom python script that performs a Gaussian smoothing of the data with $\sigma = 1.2$ pixels, followed by an argmax computation. This interactive masking of tissue compartments was performed and confirmed by 2 experienced neuroradiologists (A.B. and J.K.).

Supplemental Results

NaR:NaT and Ki-67 Proliferation Index of Tumor Cells. Statistical analysis revealed a significant correlation between the Ki-67 proliferation index of tumor cells and the mean NaR:NaT signal ratio of the whole tumor VOI (Spearman rank correlation, $S = 1963.33$, $\rho = 0.70$, $P < .001$) (On-line Fig. 7). The fact that this finding reproduces our previous observations in brain tumors of a different patient population[5] indicates this correlation is very robust.

REFERENCES

1. Smith SM. **Fast robust automated brain extraction.** *Human Brain Mapp* 2002;17:143–55 CrossRef Medline
2. Jenkinson M, Smith S. **A global optimisation method for robust affine registration of brain images.** *Med Image Anal* 2001;5:143–56 CrossRef Medline
3. Fischl B. **FreeSurfer.** *Neuroimage* 2012;62:774–81 CrossRef Medline
4. Breiman L. **Random forests.** *Machine Learning* 2001;45:5–32 CrossRef
5. Nagel AM, Bock M, Hartmann C, et al. **The potential of relaxation-weighted sodium magnetic resonance imaging as demonstrated on brain tumors.** *Invest Radiol* 2011;46:539–47 CrossRef Medline

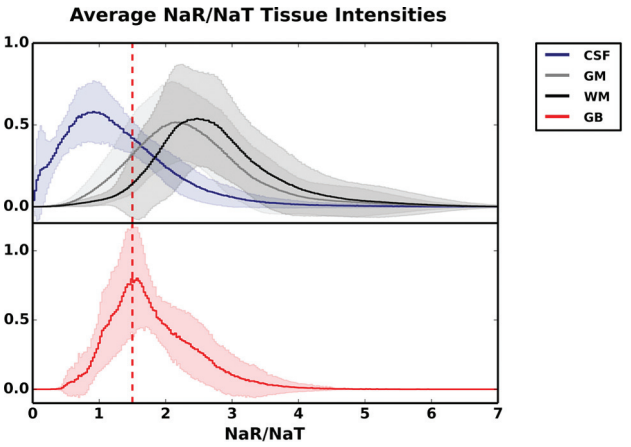

ON-LINE FIG 1. Average NaR:NaT tissue intensities. The top histogram represents the mean NaR:NaT distribution of healthy tissue, including CSF (blue), gray matter (GM) (gray), and white matter (WM) (black) for our patient cohort. At the bottom, the mean NaR:NaT distribution of the 12 patients with GB (red) is shown. Note the small standard deviation, indicated by the shaded area, for healthy and malignant tissue. This can be interpreted as a success of the normalization technique.

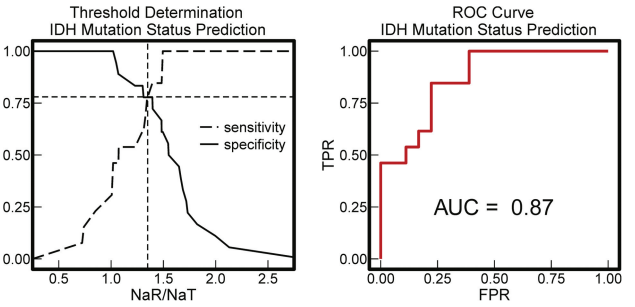

ON-LINE FIG 3. Prediction of *IDH* mutation from NaR:NaT. A logistic regression model revealed that NaR:NaT is a significant predictor of *IDH* mutation status. A combined optimization of sensitivity and specificity, that is, the intersection of the 2 measures, yields an NaR:NaT threshold of 1.35, which is used to split the cohort into groups below and above the threshold.

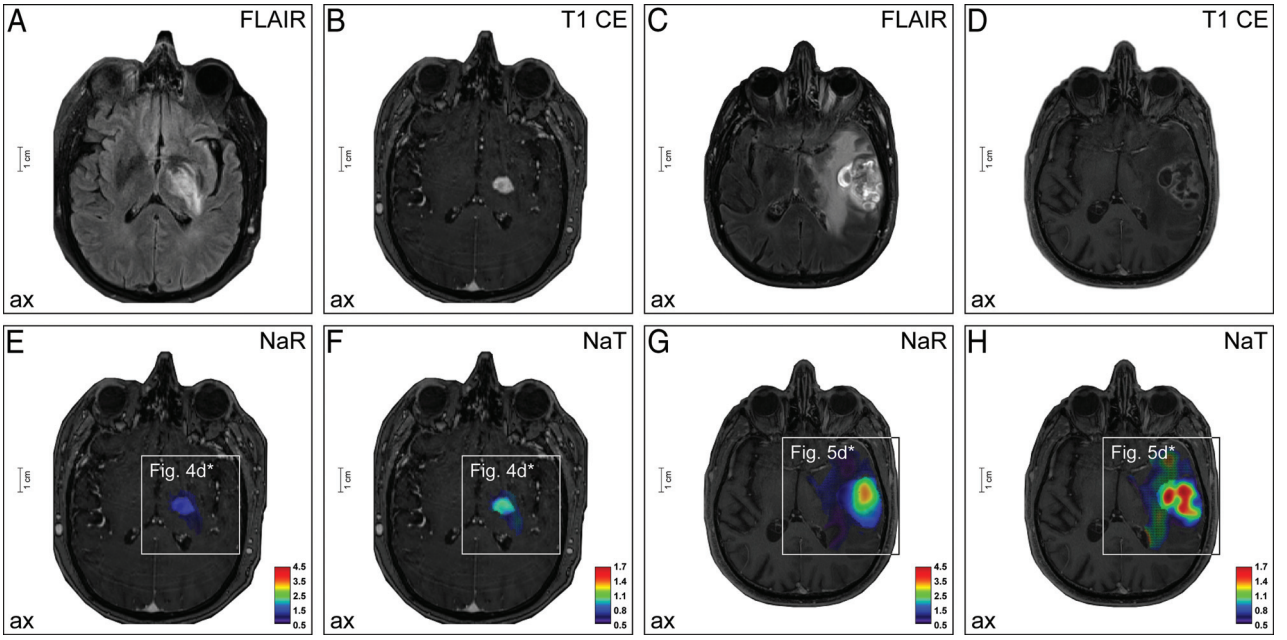

ON-LINE FIG 2. Exemplary illustration of the NaR and NaT signal behavior in low- and high-grade gliomas. T2-FLAIR and contrast-enhanced T1-weighted images (T1 CE) delineate GG (*A* and *B*) (ID no. 2, On-line Table 1) as well as GB (*C* and *D*) (ID no. 21, On-line Table 1). Na-MR imaging exhibits low NaR signals in GG (*E*) and high NaR signals in GB (*G*). The NaT signal is relatively increased in both tumors (*F* and *H*). As a result, the NaR:NaT ratio of GG (see Fig. 4*D*) is lower compared with GB (see Fig 5*D*). *Asterisk* indicates that the assigned figure is part of the main article.

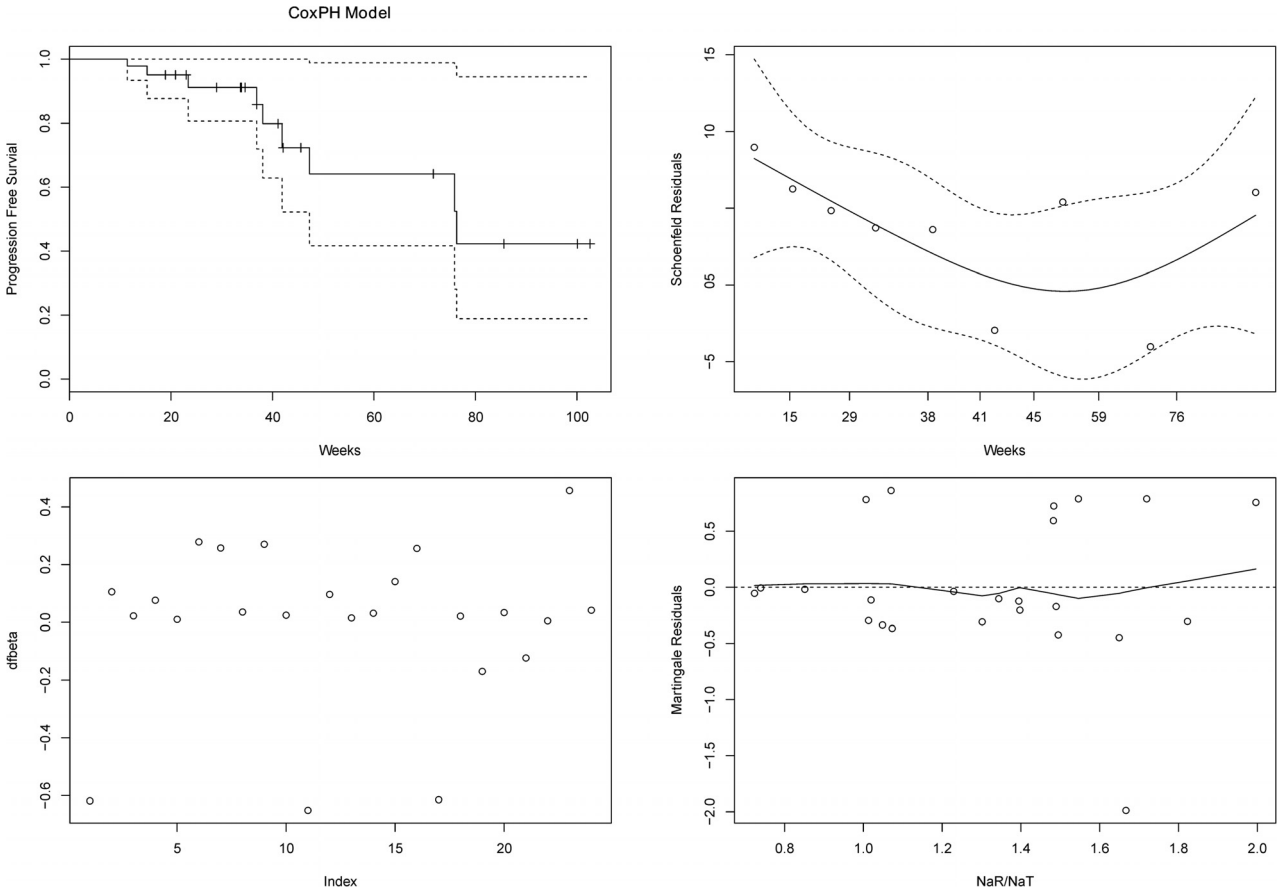

ON-LINE FIG 4. Cox PH model diagnostics. No evidence of a violation of PHs was found ($\rho = -0.43$, $\chi^2 = 1.68$, $P = .19$). The estimated survival function for patients with a hypothetical NaR:NaT of the mean NaR:NaT is shown in the upper left diagram; *dashed lines* indicate the 2-sided 95% CIs. For the Schoenfeld residuals (*dashed lines* indicate the band between the 2 standard deviations), there is no systematic deviation from the horizontal, which would indicate a violation (upper right diagram). The plot in the lower left diagram depicts beta residuals for all the patients. Three patients (ID nos. 1, 11, and 17) show residuals distinctly different from zero. Furthermore, we determined Martingale residuals to check for nonlinearity (lower right, 1 outlier [ID no. 17]). Nevertheless, a model on the patient cohort, excluding the 3 outliers, yielded significant results ($\chi^2[1] = 9.21$, $P = .002$).

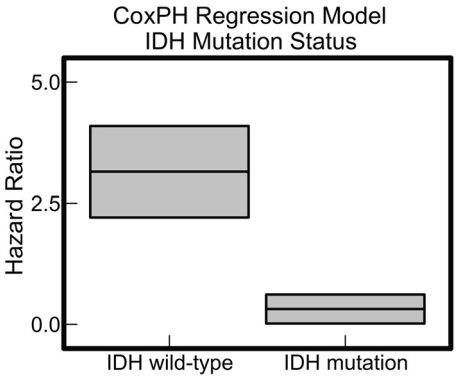

ON-LINE FIG 5. Hazard ratio of *IDH* mutation. The hazard ratio, that is, the change of hazard rate, was estimated by using a Cox PH model. Hazard rates were reliably predicted by the *IDH* mutation status. A comparison of both Cox PH models revealed that NaR:NaT is a better predictor of PFS than the *IDH* mutation status.

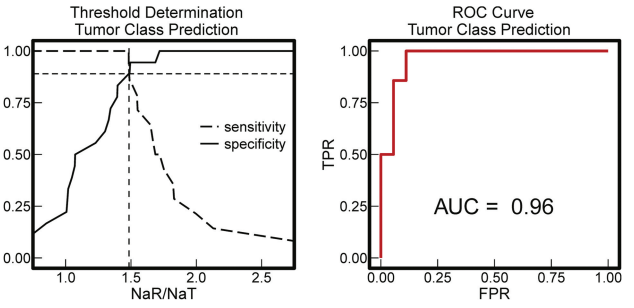

ON-LINE FIG 6. Prediction quality of tumor classification by NaR:NaT. A logistic regression model demonstrated the mean NaR:NaT of the whole tumor VOI to be significantly predictive for the binary classification of GB + metastasis vs REST. At an NaR:NaT threshold of 1.50, a specificity of 94% and a sensitivity of 86% are achieved, the corresponding area under the curve is 96%.

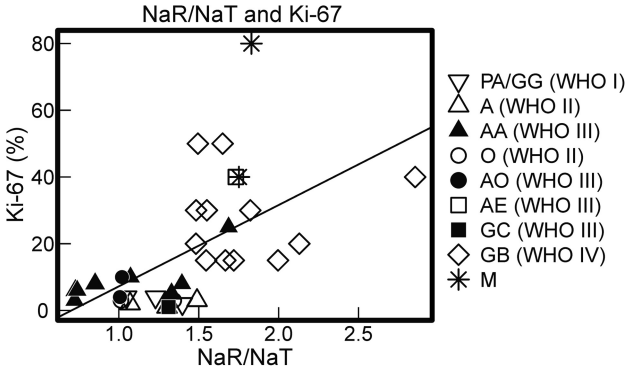

ON-LINE FIG 7. NaR:NaT and Ki-67 tumor proliferation index. Statistical analyses revealed a strong correlation between the mean NaR:NaT of the whole tumor VOI and the proliferation index Ki-67 of tumor cells. O indicates oligodendroglioma; AO, anaplastic oligodendroglioma; AE, anaplastic ependymoma; GC, gliomatosis cerebri; A, astrocytoma; M, metastasis.

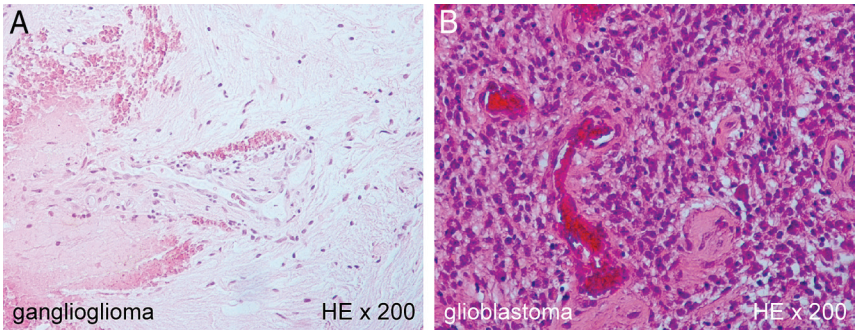

ON-LINE FIG 8. Hematoxylin-eosin staining of stereotactic biopsy tissue samples. *A*, Hematoxylin-eosin stained tissue samples of the GG confirm a low cellular tumor with nonproliferating endothelium in vessels. *B*, Histopathologic analysis of the hematoxylin-eosin stained GB specimen reveals a highly cellular tumor with vascular proliferation. The zoom factor of both microscopic images is ×200.

On-line Table 1: Patient and tumor characteristics

ID No.	Age, y	Sex	Tumor	WHO Grade	NaR:NaT Whole Tumor VOI	NaR:NaT CE Tumor VOI	PFS, weeks	*IDH* Mutation	Ki-67, %	Radiation and/or Chemotherapy
1	73	M	PA	I	1.05	0.88	102.6+	0	4	R
2	49	M	GG	I	1.40	1.26	36.9+	0	2	R
3	73	F	PA	I	1.23	1.18	20.9+	0	4	None
4	38	M	A	II	1.49	None	34.6+	1	3	T
5	69	M	A	II	1.07	None	41.9	0	2	T
6	27	M	A	II	1.30	1.43	45.6+	1	1	T
7	41	M	AA	III	0.85	0.90	29+	1	8	R
8	54	F	AA	III	0.73	None	39.6+	NI	6	R
9	28	M	AA	III	0.72	None	71.7+	1	3	R
10	65	M	AA	III	1.69	None	NI	0	25	T
11	39	M	AA	III	0.74	None	23+	1	6	R/T
12	20	F	AA	III	1.07	0.99	85.6+	1	10	R/T
13	20	M	AA	III	1.39	None	33.7+	1	8	T
14	24	F	AA	III	1.33	1.65	NI	1	5	NI
15	63	M	GB	IV	1.55	1.69	NI	0	30	R/T
16	63	F	GB	IV	2.85	2.99	NI	0	40	BSC
17	57	M	GB	IV	1.55	None	23.4	0	15	R/T
18	60	M	GB	IV	1.72	1.75	15.3	0	15	R/T
19	58	M	GB	IV	1.67	2.63	76.3	0	15	R/T
20	64	M	GB	IV	1.48	None	38.1	0	20	None
21	70	M	GB	IV	1.65	2.02	47.3	0	50	R/T
22	80	F	GB	IV	1.48	1.66	36.9	0	30	T
23	44	F	GB	IV	1.82	2.20	18.9+	0	30	R/T
24	37	M	GB	IV	2.13	2.14	NI	0	20	BSC
25	37	M	GB	IV	1.49	1.81	41.1+	1	50	R/T
26	57	M	GB	IV	2.00	2.18	11.4+	0	15	T
27	48	F	O	II	1.01	None	100.1+	1	3	R
28	30	M	O	II	1.34	None	33.9+	1	3	None
29	48	F	AO	III	1.01	None	75.9	2	4	PC
30	40	M	AO	III	1.02	1.78	42.1+	1	10	PCV
31	82	F	GC	III	1.31	None	NI	0	1	BSC
32	46	F	AE	III	1.73	1.69	NI	0	40	R/T
33	61	F	M[a]	—	1.83	2.57	NI	NI	80	R
34	79	M	M[b]	—	1.75	3.17	NI	NI	40	R

Note:—R indicates radiotherapy; T, temozolomide; NI, no information; BSC, best supportive care in patients with a Karnofsky Performance Index of <50%; O, oligodendroglioma; AO, anaplastic oligodendroglioma; PC, procarbazine and lomustine; PCV, procarbazine, lomustine, and vincristine; GC, gliomatosis cerebri; AE, anaplastic ependymoma; A, astrocytoma; M, metastasis.

[a] Metastasis of breast cancer.

[b] Metastasis of prostate cancer.

On-line Table 2: Na-MR sequence details

	Na-MR Sequence	
	NaT[a]	NaR[b]
TE, ms	0.35	0.75
TR, ms	160	185
Readout duration, ms	10	16.7
TI, ms	—	41
Nominal spatial resolution, mm^3	3.0 × 3.0 × 3.0	4.4 × 4.4 × 4.4
Acquisition time	10 min, 4 s	9 min, 52 s

Note:— — indicates not applicable.

[a] We minimized relaxation weighting by a short TE and a long TR.

[b] We measured the relaxation-weighted Na signal (NaR) by using an inversion recovery sequence that suppresses the signal of Na ions with long relaxation times as, for example, in CSF.

On-line Table 3: Pair-wise *t* tests of NaR:NaT derived from the whole tumor VOI

	t and *P* Values[a]
	GB
PA/GG	$t(30) = 2.52$, $P = .035$
A	$t(30) = 2.24$, $P = .039$
AA	$t(30) = 4.49$, $P = .001$
O	$t(30) = 2.31$, $P = .039$
AO	$t(30) = 2.93$, $P = .019$
M	$t(30) = 0.03$, $P = .976$

Note:—A indicates astrocytoma; M, metastasis.

[a] All *P* values are Benjamini-Hochberg corrected for multiple comparisons.

On-line Table 4: Pair-wise *t* tests of NaR:NaT based on the CE tumor VOI

	t and *P* Values[a]		
	AA	GB	M
GB	$t(16) = 3.42$, $P = .005$	—	—
M	$t(16) = 4.44$, $P = .001$	$t(16) = 2.41$, $P = .034$	—
PA/GG	$t(16) = 0.23$, $P = .822$	$t(16) = 3.69$, $P = .004$	$t(16) = 4.63$; $P = .001$

Note:— — indicates not applicable; M, metastasis.

[a] All *P* values are Benjamini-Hochberg corrected for multiple comparisons.